LGR4 promotes proliferation and homing via activation of the NF-κB signaling pathway in multiple myeloma

NIHAN HE[1,2], QIN YANG[3], ZHENGJIANG LI[1,2], JIAOJIAO GUO[3], CHUNMEI KUANG[3],
YINGHONG ZHU[1,2], XING LIU[1,2], XUN CHEN[1,2], FANGMING SHI[1,2],
XIANGLING FENG[4], GANG AN[5], GUOPING ZHANG[3] and WEN ZHOU[1,2]

[1]National Clinical Research Center for Geriatric Disorders, Key Laboratory for Carcinogenesis and Invasion, Chinese Ministry of Education, Furong Laboratory, Changsha, Hunan 410008, P.R. China; [2]Cancer Research Institute, School of Basic Medical Sciences, Central South University, Changsha, Hunan 410008, P.R. China; [3]Department of Hematology, Xiangya Hospital, Central South University, Changsha, Hunan 410008, P.R. China; [4]Xiangya School of Public Health, Central South University, Changsha, Hunan 410006, P.R. China; [5]State Key Laboratory of Experimental Hematology, Institute of Hematology and Blood Diseases Hospital, Chinese Academy of Medical Science and Peking Union Medical College, Tianjin 300074, P.R. China

Abstract. Multiple myeloma (MM) is a plasma cell malignancy characterized by clonal proliferation in the bone marrow (BM). Previously, it was reported that G-protein-coupled receptor 4 (LGR4) contributed to early hematopoiesis and was associated with poor prognosis in patients with MM. However, the mechanism of cell homing and migration, which is critical for MM progression, remains unclear. In the present study, cell counting, cell cycle and BrdU assays were performed to evaluate cell proliferation. Transwell assay and Xenograft mouse models were performed to evaluate cell migration and homing ability both *in vitro* and *in vivo*. I was found that overexpression of LGR4 promotes MM cell adhesion, migration and homing to BM both *in vitro,* while exacerbating osteolytic bone destruction *in vivo*. However, the LGR4 knockdown displayed the opposite effect. Further mechanistic studies demonstrated that LGR4 activated the nuclear factor kappa B (NF-κB) signaling pathway and migration-related adhesion molecule, thus promoting MM cell homing. Moreover, inhibiting the NF-κB pathway was found to suppress MM cell homing. These findings identify LGR4 as a critical regulator of myeloma cell migration, homing and tumorigenesis, offering a potential therapeutic strategy for MM treatment.

Correspondence to: Dr Wen Zhou, Cancer Research Institute, School of Basic Medical Sciences, Central South University, 110 Xiangya Road, Changsha, Hunan 410008, P.R. China
E-mail: wenzhou@csu.edu.cn

Dr Guoping Zhang, Department of Hematology, Xiangya Hospital, Central South University, 78 Xiangya Road, Changsha, Hunan 410008, P.R. China
E-mail: zhangguoping@csu.edu.cn

Introduction

Multiple myeloma (MM) is a hematologic malignancy characterized by clonal proliferation and focal proliferation of terminally differentiated plasma cells in the bone marrow (BM), which produce monoclonal immunoglobulin in the blood or urine (1). The primary clinical manifestations of MM are bone dise(ase, including osteolytic bone lesions and pathological fractures (2). Bone disease occurs in up to 90% of patients. MM cell proliferation is highly dependent on the BM microenvironment (BMME) and its adhesive interactions with extracellular matrix components, including fibronectin and collagen (3). Enhanced adhesion of MM cells promotes their homing to the BM (4), followed by malignant proliferation that exacerbates bone destruction (5). Therefore, understanding the mechanisms of MM cell proliferation, migration and homing into the BM is essential for developing new strategies for MM treatment.

As the fourth member of the G protein-coupled receptors, LGR4 is involved in multiple physiological and pathological processes, including embryonic development (6), stem cell maintenance (7), bone remodeling (8) and tumorigenesis. A previous research by the authors has demonstrated that LGR4 plays a role in regulating the number of fetal liver hematopoietic stem cells (9). It has been reported that LGR4-deficient mice exhibit multiple organ defects, such as eye (10), bone (8) and reproductive organs (11), and exhibit abnormal energy metabolism (12). Additionally, LGR4 is known as a key regulator of osteoblast and osteoclast differentiation (8). The high expression of LGR4 has been associated with poor prognosis of multiple cancers. LGR4 is upregulated in cancer and is involved in regulating tumorigenic processes. LGR4 promotes cell migration, invasion and proliferation in prostate, colorectal and cervical cancers (13). In colorectal cancer, LGR4 directly induces cell ferroptosis and drug resistance through Wnt-βcatenin signaling (14). Moreover, LGR4 enhances osteoclastic premetastatic niche formation

and promotes bone metastasis in breast cancer cells through the Gαq and β-catenin signaling pathways (15). These findings suggest potential crosstalk between tumor cell receptors and BMME during cancer progression. Additionally, it has been indicated that the LGR4/R-spondin axis plays a crucial role in activating Wnt signaling in MM (16). LGR4 is highly expressed in patients with MM, promoting MM cell proliferation (17). A previous study has reported that LGR4 can activate the NF-κB signaling pathway. It has been reported that activated NF-κB signaling enhances the ability of hematopoietic stem cell homing (18). However, the unique function and mechanism of LGR4 in MM remain unclear. It remains unclear whether LGR4, a membrane protein, increases the interaction between MM cells and BMME, thereby promoting cell homing to BM and accelerating MM progression.

In the present study, it was demonstrated that LGR4 was positively associated with cell adhesion molecules, and its high expression was associated with poor prognosis in MM. It was aimed to investigate the effects of LGR4 on MM progression through its role in cell adhesion, migration and BM homing both *in vitro* and *in vivo*. The present findings suggest that targeting LGR4 can offer a potential therapeutic strategy for MM treatment.

Materials and methods

Clinical samples. BM samples derived from healthy donors (HD; n=5) and newly diagnosed patients with MM (n=9) were obtained from Xiangya Hospital, the Second Xiangya Hospital of Central South University (Changsha, China), from January 2020 to June 2023. CD138+ plasma cells were isolated by using anti-human CD138 magnetic beads (Miltenyi Biotec GmbH) and incubated in 4˚C for 15 min with mono-cytes isolated from BM samples using lymphocyte separation medium (cat. no. LTS1077; TBD; https://www.tbdscience.com/). The patients with MM enrolled in the present study were newly diagnosed. International Myeloma Working Group criteria (19) were processed by hematologists for the diagnosis of MM. Patients with monoclonal gammopathy of undetermined significance (MGUS) and smoldering MM were excluded, together with patients with MM combined with other diseases. The clinical information of the enrolled patients with MM in the present study is included in Table SI. The present study was approved by Cancer Research Institute Review Board of Central South University (Changsha, China).

Cell culture. The human MM cell lines ARP1 (20), KMS28-BM (21), KMS28-pleural effusion (PE) (20) and OCI-My5 (20,22), were utilized to explore the function of LGR4 in MM. Cell lines were cultured in Roswell Park Memorial Institute (RPMI)-1640 medium (Gibco; Thermo Fisher Scientific, Inc.) supplemented with 10% fetal bovine serum (FBS; cat. no. FSP500; Shanghai ExCell Biology, Inc.) and 1% penicillin and streptomycin (P/S; Gibco; Thermo Fisher Scientific, Inc.). The cell lines have been used in previous studies (20,22). The human MM cell line OCI-T3rd-luc (derived from OCI-My5-luc) was established by our group using tail vein injection into NCG mice with three rounds of homing transplantation and enriched from BM. KMS28-BM (21) and KMS28-PE cells are the paired cell lines originated from BM

and PE of MM patients with immortalization. The human BM stromal cell line HS5 (a gift from Dr. Jiaxi Zhou, Institute of Hematology, Chinese Academy of Medical Sciences) was maintained in DMEM low glucose supplemented with 10% FBS and 1% P/S.

Reagents and antibodies. Reagents included QNZ (cat. no. EVP4593; Selleck Chemicals) and doxycycline (DOX; cat. no. 24390-14-5; MilliporeSigma). The antibodies were as follows: Anti-LGR4 (1:1,000; cat. no. A12657; for western blotting), anti-β-actin (1:5,000; cat. no. AC004), anti-nuclear factor kappa B (NF-κB) 2 (1:1,000; cat. no. A19605), anti-P-NF-κB2-S866 (1:1,000; cat. no. Ap0418), anti-IκBα (1:1,000; cat. no. A19714), anti-P-IκBα-S36 (1:1,000; cat. no. A191714), anti-Snail (1:1,000; cat. no. A5243) and anti-TNFRSF1B (1:1,000; cat. no. A13556) were all obtained from ABclonal Biotech Co., Ltd. Anti-GAPDH (1:5,000; cat. no. 10494-1-AP), anti-MUC2 (1:1,000; cat. no. 27675-1-AP), anti-Caspase (1:1,000; cat. no. 319677-1-AP) and anti-Zinc Finger E-Box Binding Homeobox 1 (ZEB1; 1:1,000; cat. no. 21544-1-AP) were all obtained from Proteintech Group, Inc. Anti-poly-(ADP-ribose) polymerase (PARP) antibody (1:1,000; cat. no. 9532), anti-cleaved caspase 3 antibody (1:1,000; cat. no. 9664) and anti-Vimentin (1:1,000; cat. no. D21H3) were obtained from Cell Signaling Technology, Inc. Anti-N-cadherin (1:800; cat. no. WL011047) was obtained from Wanleibio Co., Ltd. PE anti-human CD138 (cat. no. 352306) was obtained from BioLegend, Inc. and CXCR12 (cat. no. 350-NS) from R&D Systems, Inc.

Vectors and transfections. LGR4-overexpression (LGR4-OE) constructs were constructed by cloning LGR4 cDNA into a pSIN-EF2-Puro (23) lentiviral vector using EcoRI (cat. no. R3101S; New England Biolabs) and BamHI (cat. no. R3136S; New England Biolabs). LGR4-knockdown constructs using two pairs of short hairpin RNA sequences (shRNA1 and shRNA2) were ligated into a pLKO-tet-on lentiviral vector. Aim Lentiviruses (5 μg) were packaged in 293T cells (a gift from Dr. Rong Chang, Kunming Institute of Zoology, the Chinese Academy of Sciences) using pMD2G (1.25 μg) and psPAX2 (3.75 μg) helper vectors and poly-brene (8 μg/ml)-mediated transduction (cat. no. H9268-5G; MilliporeSigma). After 60 h the 10 ml virus was collected and 1ml virus was used to transfect 1x10⁶ ARP1 or OCI-My5 cell lines in 1 ml medium. A total of 48-72 h after the transfection, puromycin (1 μg/ml) was added to screen the positive cells. The final concentration of siRNA transfection was 50 nM. Transient transfection was performed using a Nefect DNA Transfection reagent (cat. no. TF20121201; Neofect; http://www.neofect.cn/) according to the specification. All primer and siRNA sequences are listed in Tables SII and SIII.

Western blotting. Western blot analysis was performed as previously described (20). Proteins were separated by 10% sodium dodecyl sulfate-polyacrylamide gel elec-trophoresis (SDS-PAGE) and transferred to a 0.45-μm polyvinylidene fluoride membrane. The blots were then probed with specific primary antibodies overnight at 4˚C, followed by HRP-conjugated secondary antibodies incubation for 1 h at room temperature (RT). Protein signals were developed with

SuperSignalTM West Femto Maximum Sensitivity Substrate (Thermo Fisher Scientific, Inc.).

Reverse transcription-quantitative PCR (RT-qPCR). To detect mRNA expression in MM cells, RT-qPCR was performed as previously described (22). Total RNA was extracted using TRIzol® (cat. no. 15596026; Thermo Fisher Scientific, Inc.) according to the manufacturer's protocol. Total RNA was reverse transcribed using the SuperScript™ II Reverse Transcriptase kit (cat. no. 18064071; Thermo Fisher Scientific, Inc.). qPCRs were performed by using ABsolute qPCR SYBR Green Mixes (cat. no. AB1163A; Thermo Fisher Scientific, Inc.) according to the manufacturer's protocol. All primer sequences are listed in Table SIV.

Immunofluorescence analysis. A total of $4x10^4$ CD138+ cells were spun down on glass slides and then fixed with methanol for 15 min at 20°C. Diluted LGR4 antibodies (1:200) and ZEB1 antibodies (1:200) were placed on glass slides and incubated overnight at 4°C. Then, the cells were incubated with secondary antibodies (1:1,000) conjugated with Goat anti-Rabbit Alexa Fluor™ 488 (cat. no. A-11008; Thermo Fisher Scientific, Inc.) or Goat anti-Mouse Alexa Fluor™ 594 (cat. no. A-11012; Thermo Fisher Scientific, Inc.) for 2 h at RT (protected from light). Nuclei were labeled with 4',6-diamidino-2-phenylindole (DAPI, 1 mg/ml; 1:5,000) (cat. no. S2110; Beijing Solarbio Science & Technology Co., Ltd.). Fluorescence was observed under a Leica fluorescence microscope. The fluorescence intensity was quantified using ImageJ 1.54 software (National Institutes of Health).

Cell proliferation and viability assay. To determine cell proliferation, MM cells were plated in 24-well plates with 5,000 cells per well by counting alive cells after trypan blue exclusion. Cell numbers were counted using a cell counting chamber for six days. To determine cell viability, MM cells were plated in 96-well plates at a density of 5,000 cells per well. The cells were treated with QNZ for 48 h and counted using Cell Counting Kit-8 (cat. no. B34302; Bimake). For each well, 10 μl of reagent was added, followed by incubation at 37°C for 2-3 h. The optical density (OD) was measured at 450 nm . Each test was repeated three times. IC_{50} was calculated using GraphPad Prism 9 software.

Soft-agar colony formation assay. Soft agar colony formation assay was performed as previously described (22). The colonies were treated with RPMI-1640 complete medium in the presence or absence of DOX twice every week. One colony was defined if >50 cells were observed. Plates were imaged, and colonies were enumerated using ImageJ software.

Flow cytometry. For BrdU assay, cells were starved with 2% FBS-RPMI1-640 for 12 h and recovered in 10% FB-RPMI1640 for 24 h for cell synchronization. Cells were labeled with BrdU in culture medium for 1 h. All procedures followed the standard protocol with the allophycocyanin (APC) BrdU Flow Kit (cat. no. 552598; BD Biosciences). Cell cycle progression was determined by propidium iodide (PI) staining. Cells were fixed in 75% ethanol at -20°C overnight and incubated with PI/RNase Staining Buffer (cat. no. 550825; BD Biosciences)

for 15-20 min at RT (protecting the cells from light). For apoptosis assay, cells were labeled by APC-conjugated Annexin V and PI/7-aminoactinomycin D (cat. no. A7313020; Shanghai Yeasen Biotechnology Co., Ltd.) according to the manufacturer's protocol. Stained cells were analyzed by flow cytometry (DxP Athena B4-R2; Cytek Biosciences) and analyzed with FlowJo 10.0 software (FlowJo LLC).

Cell migration, invasion and homing assay. The Transwell assay was performed using the Transwell chambers (Corning, Inc.) with a filter membrane (aperture 8 μm). For the migration assay, the chemoattractant was 10% FBS. The invasion experiment required the addition of Matrigel to the upper chamber and incubation at 37°C for 2 h, followed by the same steps as the migration assay. The chemoattractant of the cell homing assay was CXCR12 (40 ng/ml). Cells were starved with 2% FBS-RPMI1640 for 12 h. Then $5x10^5$ cells/400 μl serum-free medium/well were inoculated into the upper chamber, and 600 μl/well medium with chemoattractant was added into the lower chamber. After incubation in 37°C for 24 h, the migratory cells in the lower chamber were harvested and counted through flow cytometry. After removing the cells in the upper chambers, chambers were stained with 0.2% crystal violet (CV) for 20 min. The filter membrane was cut and placed on the glass slide for counting using a Leica light microscope.

Cell adhesion assay. A co-culture system was used to detect the direct adhesion ability of MM cells. 96-well plates were incubated at 37°C with fibronectin (FN; 50 μg/ml; 100 μl/well; cat. no. 354008; Corning, Inc.) or seeded HS5 cells ($2x10^4$ cells/well) overnight. LGR4-OE or LGR4-knockdown ARP1 and OCI-My5 were harvested and resuspended with serum-free RPMI-1640 medium, seeded with $1x10^5$ MM cell/100 μl into 96-well plate. To detect the adhesion ability of MM cells after being treated with QNZ for 48 h, MM cells were harvested and seeded into the 96-well pre-coated with FN or HS5 cells. After co-culture for 4 h, non-adherent MM cells were removed. Adherent cells were stained with 0.2% CV for 2 h at RT. Superfluous CV was washed off with distilled water, and the plates were dried overnight at RT. The dye was dissolved with 2% SDS for 2 h on the shaking platform, and the plates were measured at 570 nm using a microplate reader. The optical densities (ODs) from HS5s cultured alone were tested as background absorption.

Homing assay and Xenograft mouse models of MM. All animal experiments were performed in accordance with the guidelines of the Institutional Animal Care and local Veterinary Office and Ethics Committee of the Animal Center of Hunan Normal University School of Medicine (approval no. D2021013; Changsha, China). The SPF housing conditions were maintained at 20-26°C, with relative humidity at 40-70% and a 12/12-h light/dark circadian rhythm. OCI-My5 cells ($1x10^6$ cells in 200 μl PBS) were injected by tail vain intravenously into 8 weeks-old female NCG mice (n=22; weight, 19-24 g) (NOD/ShiLtJGptPrkdc^{em26Cd52}Il2rg^{em26Cd22}/Gpt, GemPharmatech). MM progression in the mice was monitored by measuring the tumor burden through live imaging. Homing assay of injected MM cells to the BM was measured by flow cytometry. Mice were euthanized using sodium pentobarbital

at a dose of 100 mg/kg via intraperitoneal injection, and living imaging of leg bones was performed at week 6. Homing MM cells were flushed out of the BM with 1X PBS. After lysis of the erythrocyte lysate (ACK lysis Buffer; cat. no. SL1070; Coolaber science & technology Co., Ltd.), the cells were labeled with PE-anti-human CD138 (1:100; cat. no. 352306; BioLegend, Inc.). Flow cytometry was used to analyze the proportion of the homing cells to BM.

Radiography and micro-computed tomography (micro-CT). Micro-CT scanning was performed as previously described (22). The mouse tibia was fixed in 4% paraformaldehyde (PFA) in 4°C for 48 h. Tibia scans were performed by High-resolution Micro-CT (Skyscan 1176; Bruker, https://www.bruker.com/zh.html?ao=1) at a resolution of 6.5 μm per pixel. Measuring the bone parameters, including trabecular bone volume fraction (Tb. BV/TV), trabecular number (Tb.N), trabecular thickness (Tb.Th) and trabecular separation (Tb.Sp). These bone parameters were analyzed using DataViewer 1.4.1.9 (CTAn version 1.11) and (μCTVol version 2.2; (both from Bruker Corporation).

Tartrate-resistant acid phosphatase (TRAP) staining. The mouse tibia was fixed in 5 ml of 4% PFA solution at 4°C overnight and then decalcified the tibia in 10 ml of 0.5 M EDTA at 4°C for 24 h. Paraffin sections (6 μm) were stained with (TRAP; cat. no. 387a-1KT; MilliporeSigma). Images of TRAP were obtained through a light microscope (Keyence Corporation).

Immunohistochemistry (IHC). The experimental mice tibia was fixed with PFA in 4°C, embedded in paraffin following gradient ethanol dehydration, and sliced into 3 μm for IHC. The slides were dewaxed with xylene, rehydrated, and subjected to antigen retrieval treatment using an IHC kit (cat. no. KIT-9720; MXB Biotechnologies; http://www.maxim.com.cn/sitecn/myzhjcxthsjh/981.html). Subsequently, the slides were incubated with anti-CD138 antibody at a 1:400 dilution overnight at 4°C. Next, the slides were incubated in 25°C with HRP-conjugated antibody (Reagent 3 in IHC kit) and stained with 3,30-diaminobenzidine tetrahydrochloride hydrate (DAB) for 3 min. Finally, cell nuclei were counterstained with hematoxylin.

RNA sequencing (RNA-seq) and analysis. Total RNA was extracted from MM cells using TRIzol (cat. no. 15596018CN; Invitrogen; Thermo Fisher Scientific, Inc.), and its quality and quantity were assessed using a Fragment Analyzer (Agilent Technologies, Inc.). Library preparation was performed using Optimal Dual-mode mRNA Library Prep Kit (BGI; https://www.bgi.com/). The loading concentration of the final library is 300g/lane quantified by Qubit (Thermo Fisher Scientific, Inc.). Sequencing was performed on T7 platform (BGI) using paired-end 150-base reads are generated. MM cell lines, including OCI-EV, OCI-LGR4-OE, OCI-Ctrl and OCI-LGR4-shRNA1, were used for RNA-seq. Gene set enrichment analysis (GSEA) enrichment from differentially expressed genes between OCI-EV and OCI-LGR4-OE was performed using clusterProfiler_4.2.2 (24) function of R language, and the threshold was set as P<0.05.

Statistical analysis. Data were analyzed and represented using GraphPad Prism software (version 9; Dotmatics). All data are presented as the mean ± standard deviation (SD). The statistical significance of the data was determined using the two-tailed unpaired Student's t-test, one-way or two-way ANOVA with Tukey or Dunnett post-hoc test, or Kruskal-Wallis test. Overall survival was measured using the Kaplan-Meier method, and the log-rank test was used for group comparison based on GraphPad Prism 9 software. The statistical significance of the data in the Table SVI was determined through the Fisher-Freeman-Hanlton test. Each experiment was performed three times. The analysis of the Gene Expression Programming database utilized dataset GSE2658 and GSE24080, accessed from the GEO database (https://www.ncbi.nlm.nih.gov/geo/). *P<0.05 was considered to indicate a statistically significant difference.

Results

High expression of LGR4 is associated with cell adhesion and links to poor prognosis in MM. To identify the role of LGR4 in MM, the dataset GSE2658 (25) was analyzed, which contains data from 22 HD, 44 patients with MGUS and 351 newly diagnosed patients with MM. The analysis revealed a gradual increase in LGR4 expression (Fig. S1A). Higher expression of adhesion-associated molecules was observed in patients with MM compared with both HD and MGUS on the dataset GSE2658, same as LGR4 (Fig. 1A). These results were further validated using immunofluorescence in CD138+ cells derived from HD (n=5) and patients with MM (n=9) (Fig. S1B). The results confirmed a higher expression of LGR4 in MM, consistent with previous studies (16,17).

The focal proliferation of MM cells in the BM is a hallmark of MM, where increased adhesion enhances cell homing (9). To investigate whether LGR4 influences adhesion and homing, the association of LGR4 and adhesion-associated molecules was examined. Pearson's correlation heatmap analysis exhibited a positive correlation between LGR4 and adhesion-associated molecules (Fig. 1B). Subsequently, RNA-seq data of OCI-T3rd-luc cells revealed significant upregulation of LGR4 and adhesion genes compared with OCI-My5-luc cells (Fig. 1C). Additionally, the high expression of LGR4 along with adhesion genes was verified using RNA-seq data from paired KMS28-BM and KMS28-PE cell lines (Fig. 1D). Among the positive correlated gene, it was found that ZEB1, a transcription factor associated cell adhesion (26), is associated with worse overall survival; as MM patients with LGR4highZEB1high (n=85) exhibited significantly worse overall survival (P=0.068) (Figs. 1F and S1F). Furthermore, ZEB1 expression was significantly increased in KMS28-BM compared with KMS28-PE cells, at both mRNA (Fig. S1D) and protein levels (Figs. 1E and S1C-E). These results suggested that LGR4 is associated with cell adhesion and promoted MM cell homing to the BM. In summary, high expression of LGR4 is associated with increased cell adhesion and is associated with poor prognosis in MM.

LGR4 overexpression promotes cell adhesion, migration and homing in MM cells in vitro. To explore whether high expression of LGR4 promotes MM progression, LGR4 was
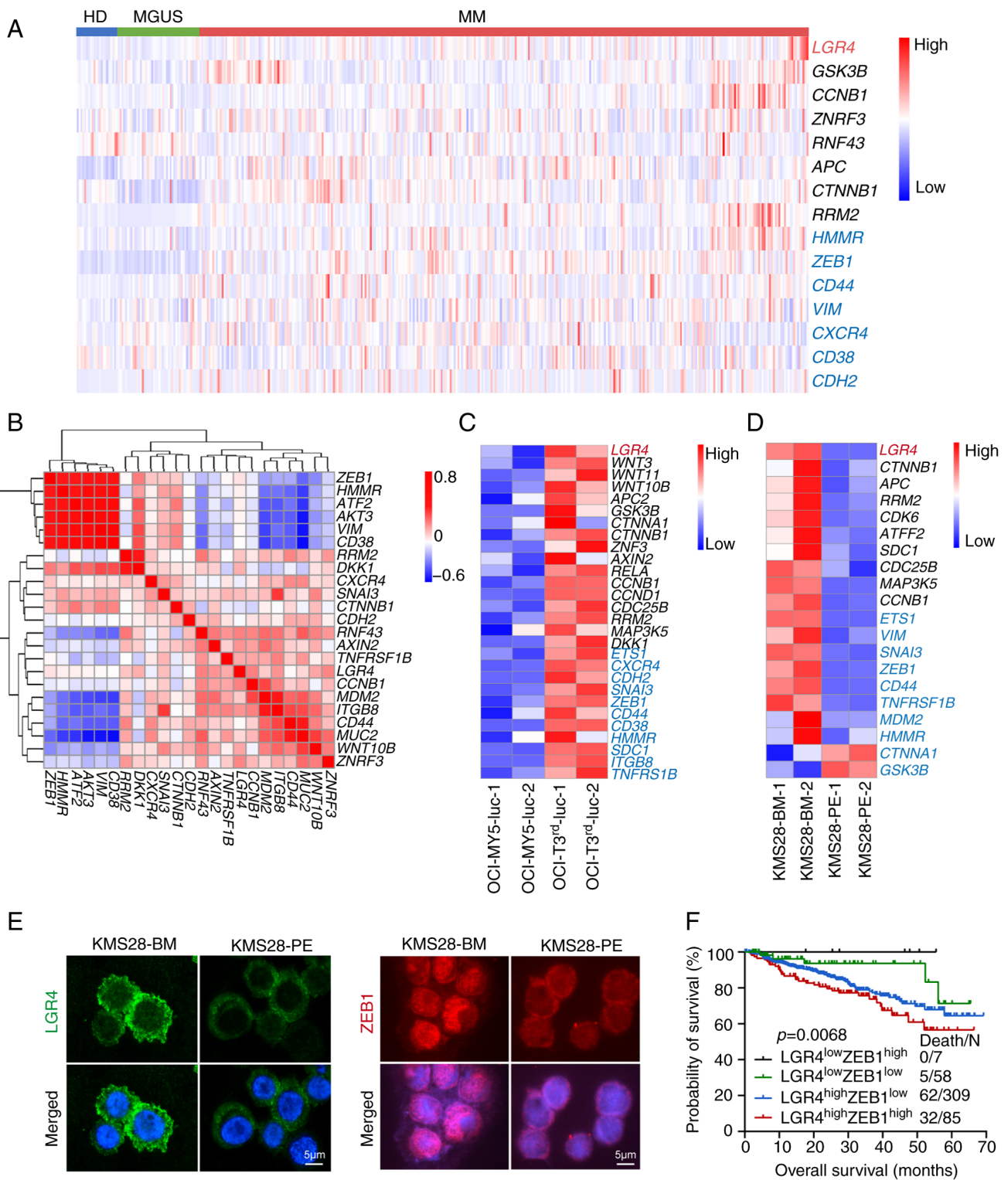
Figure 1. High expression of LGR4 is associated with cell adhesion and poor prognosis in multiple myeloma. (A) Gene expression heatmap of LGR4 (Red) and Wnt/β-catenin signal related genes (Black), Cell adhesion associated genes (Blue) in CD138+ cells from HD (n=22), MGUS (n=44) and MM (n=351). (B) Pearson's correlation analysis of the relationship between LGR4 and cell adhesion genes. Red for positive, blue for negative. (C) Gene expression heatmap of OCI-My5 and OCI-T3rd-luc with LGR4 (Red), Wnt/β-catenin signal genes (Black), Cell adhesion associated genes (Blue). (D) Gene expression heatmap of KMS28-BM and KMS28-PE with LGR4 (Red), Wnt/β-catenin signal genes (Black), Cell adhesion associated genes (Blue). (E) Representative images of immunofluorescence images of LGR4 and ZEB1 protein expression in KMS28-BM and KMS28-PE. Scale bars, 50 μm. (F) Kaplan-Meier analyses of overall survival in MM patients with LGR4^{low}ZEB1^{low} (n=58), LGR4^{low}ZEB1^{high} (n=7), LGR4^{high}ZEB1^{low} (n=309) and LGR4^{high}ZEB1^{high} (n=85) from GSE2658. HD, healthy donors; MGUS, monoclonal gammopathy of undetermined significance; MM, multiple myeloma; BM, bone marrow; PE, pleural effusion; ZEB1, Zinc Finger E-Box Binding Homeobox 1.

overexpressed in both ARP1 and OCI-My5 using lentivirus (Figs. 2A, S2A and B). LGR4 overexpression significantly

enhanced cell proliferation, as indicated by the growth curve assay (Fig. S2E), a higher proportion of BrdU-positive cells by

the BrdU incorporation assay (Figs. 2B and S2C) and a marked increase in colony formation in the soft-agar colony formation assay (Fig. 2C) compared with the EV group. Additionally, cell cycle assays indicated that LGR4 overexpression increased the percentages of both the S phase and G2/M phase in ARP1 and OCI-My5 cells (Fig. S2D). The aforementioned results confirmed that LGR4 overexpression promotes the proliferation of MM cells.

Next, the effect of LGR4 was examined on the migration, invasion and homing abilities of MM cells. A Transwell assay using different chemo-attractants was performed to assess cell migration (Fig. 2D). The results indicated that LGR4 overexpression significantly promoted cell migration and invasion, which was quantified by counting migratory cells (Fig. 2E and F). Additionally, a cell homing assay using CXCR12, a chemokine known to induce immune cell homing to BM (27), demonstrated that more cells homed to the BM in the LGR4-OE group (Fig. 2G). As previously reported, FN acts as a connection between cells and matrix (26), and the HS5 cell line mimics the bone marrow stromal cells (BMSCs), promoting MM cell proliferation and adhesion (28). To determine whether LGR4 improves the interaction between MM cells and the BMME, a cell adhesion co-culture assay was performed using FN and HS5 cells (29)(Fig. 2H). The OD value at 570 nm indicated a direct increase in adhesion to both FN and HS5 in the LGR4-OE group (Fig. 2I). Even though in ARP1-LGR4-OE cells was observed increase tend of adhesion (P=0.06), which may cause by the complex genetic characteristics such as *TP53*[del] (30), the aforementioned results demonstrated that LGR4-OE enhances the cell homing and adhesion ability in MM cells.

LGR4 knockdown impairs cell proliferation, adhesion, migration and homing in MM cells in vitro. To further investigate the function of LGR4 on adhesion, migration and homing of MM cells, two shRNA sequences (shRNA1 and shRNA2) targeting *LGR4* were designed. A DOX-inducible lentiviral expression system expressing LGR4 shRNA was used to knock down LGR4 in MM cell lines. LGR4 knockdown was confirmed at both mRNA and protein levels (Figs. 3A, S3A and C). Among these, LGR4-shRNA1 silencing was confirmed to be more effective. Growth curves indicated that LGR4 knockdown significantly inhibited proliferation in MM cells following DOX induction (Fig. S3B). Additionally, the proportion of BrdU-positive cells in the LGR4-shRNA1 groups was significantly lower than in the control group (Fig. 3B and C). The colony formation of LGR4-shRNA1 cells exhibited a significant inhibition (Fig. 3D). Cell cycle assays revealed that LGR4 silencing decreased the proportion of cells in the S and G2/M phases in both ARP1 and OCI-My5 (Fig. S3D). Furthermore, the proportion of Annexin-V-positive cells was significantly increased (Fig. S3E), and cleaved caspase 3 and PARP were significantly upregulated in the LGR4-knockdown group (Fig. S3F and G), indicating that LGR4-knockdown induced apoptosis in MM cells. These results suggested that LGR4-knockdown inhibited the proliferation and induced apoptosis in MM cells.

Next, Transwell migration and invasion assays revealed that LGR4-knockdown reduced both migration and invasion, with a corresponding decrease in the number of migratory cells

(Fig. 3E and F). Additionally, LGR4-knockdown decreased the homing of MM cells induced by the BM chemokine CXCR12, as confirmed by statistical analysis (Fig. 3G). Using cell-adhesion co-cultured assay, the absorbance at 570 nm exhibited that LGR4-knockdown suppressed the adhesion ability of MM cells to FN and BMSCs (Fig. 3H and I). The aforementioned results confirmed that LGR4-mediated interaction between malignant plasma cells and BMME is crucial for cell adhesion and homing to BM niches.

LGR4 overexpression promotes cells' homing to BM and MM progression in vivo. To further explore the role of LGR4 in MM cell homing *in vivo,* OCI-My5 cells with LGR4-OE were generated and injected through the tail vein into NCG mice. MM cells are typically home to BM, where they proliferate and cause symptoms, including hindlimb paralysis (31). Tumor burden was monitored through whole-animal live imaging, evaluating the proportion of human MM cells in BM and their homing efficiency (Fig. 4A). Compared with the control mice, the LGR4-OE mice significantly demonstrated an increased tumor-associated luminescence intensity at weeks 4 and 6 (Fig. 4B and C). LGR4-OE mice exhibited 60% of paralysis, while control mice had no expression at week 6 (Fig. S4). Due to reaching the humane endpoint, the mice were euthanized at week 6. Flow cytometric analysis revealed that LGR4 overexpression significantly increased the proportion of homing MM cells in the BM. As a result, LGR4-OE significantly increased the proportion of human MM cells (AVG 55%) in the BM compared with the control mice (AVG 23.8%) (Fig. 4D).

Since MM cell homing and proliferation within the BM are key drivers of bone disease (21), bone health was further assessed by evaluating bone fractures and CD138 immunostaining. Micro-CT scanning was used to detect bone damage, finding that LGR4-OE had markedly more severe trabecular bone loss compared with the control mice (Fig. 4E). Quantitative bone microstructure parameters exhibited that LGR4-OE in mice had a lower BV/TV and Tb.N, while Tb.Sp was markedly higher compared with the controls (Fig. 4F). Consistent with these results, TRAP staining indicated the increased positive osteoclast number in the LGR4-OE mice femora compared with control mice (Fig. 4G and I). Moreover, plasma cell morphology was clearly visible at x80 magnification and exhibited enrichment in LGR4-OE mouse bones (Fig. 4G). CD138 immunostaining revealed the increased plasma cell number in the LGR4-OE mice compared with the control (Fig. 4H and J). Additionally, the potential association between LGR4 expression and clinical characteristics was assessed, using the GSE24080 dataset. It was found that LGR4 expression correlated strongly with the percentage of plasma cells in the BM (P=0.037), and the number of magnetic resonance imaging (MRI)-defined focal lesions (P=0.019) (Table SVI). These findings suggest that high expression of LGR4 is linked to myeloma cell homing, promotes bone destruction and contributes to malignant progression in patients with MM. In summary, these results demonstrated that overexpression of LGR4 enhances MM cell homing to the BM and accelerates disease progression.

Cell-adhesion association genes and NF-κB signaling pathway are upregulated in LGR4-OE MM cells. To further understand
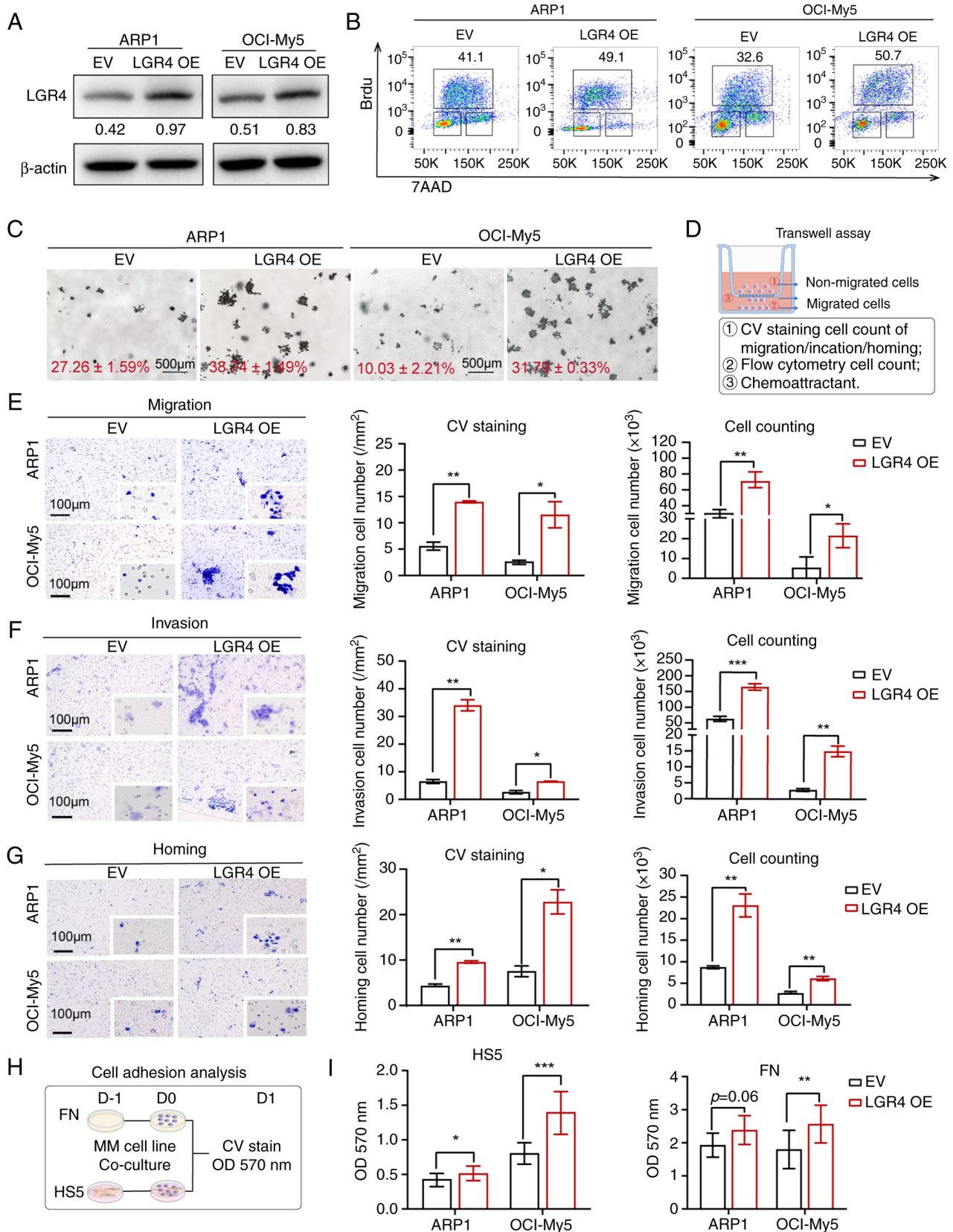
Figure 2. LGR4 overexpression promotes cell adhesion, migration and homing in MM cells *in vitro*. (A) Western blots of LGR4-OE in ARP1 and OCI-My5 MM cell lines, compared with EV. (B) Representative flow cytometry dot plots of the number of BrdU-positive cells. (C) Representative images of clonogenic analysis in ARP1-EV, ARP1-LGR4-OE, OCI-EV and OCI-LGR4-OE cells. Scale bars, 500 μm. (D) Schematics of Transwell experiments. (E) Transwell migration assays were conducted with LGR4-OE ARP1 and OCI-My5 cells. The quantification of the number of migratory cells is presented in the column graph. Scale bars, 100 μm. (F) Matrigel invasion assays were conducted with LGR4-OE ARP1 and OCI-My5 cells. The quantification of the number of invasive cells is presented in the column graph. Scale bars, 100 μm. (G) Transwell cell homing assays conducted with LGR4-OE ARP1 and OCI-My5 cells. The quantification of the number of homing cells is presented in the column graph. Scale bars, 100 μm. (H) Schematic of cell adhesion assay. (I) Adhesion assay of LGR4-OE ARP1 and OCI-My5 co-cultured with HS5 cells or FN. Statistical analyses were performed using Student's t-test. *P<0.05, **P<0.01 and ***P<0.001. LGR4-OE, LGR4 overexpression; MM, multiple myeloma; EV, empty vector; FN, fibronectin; CV, crystal violet.
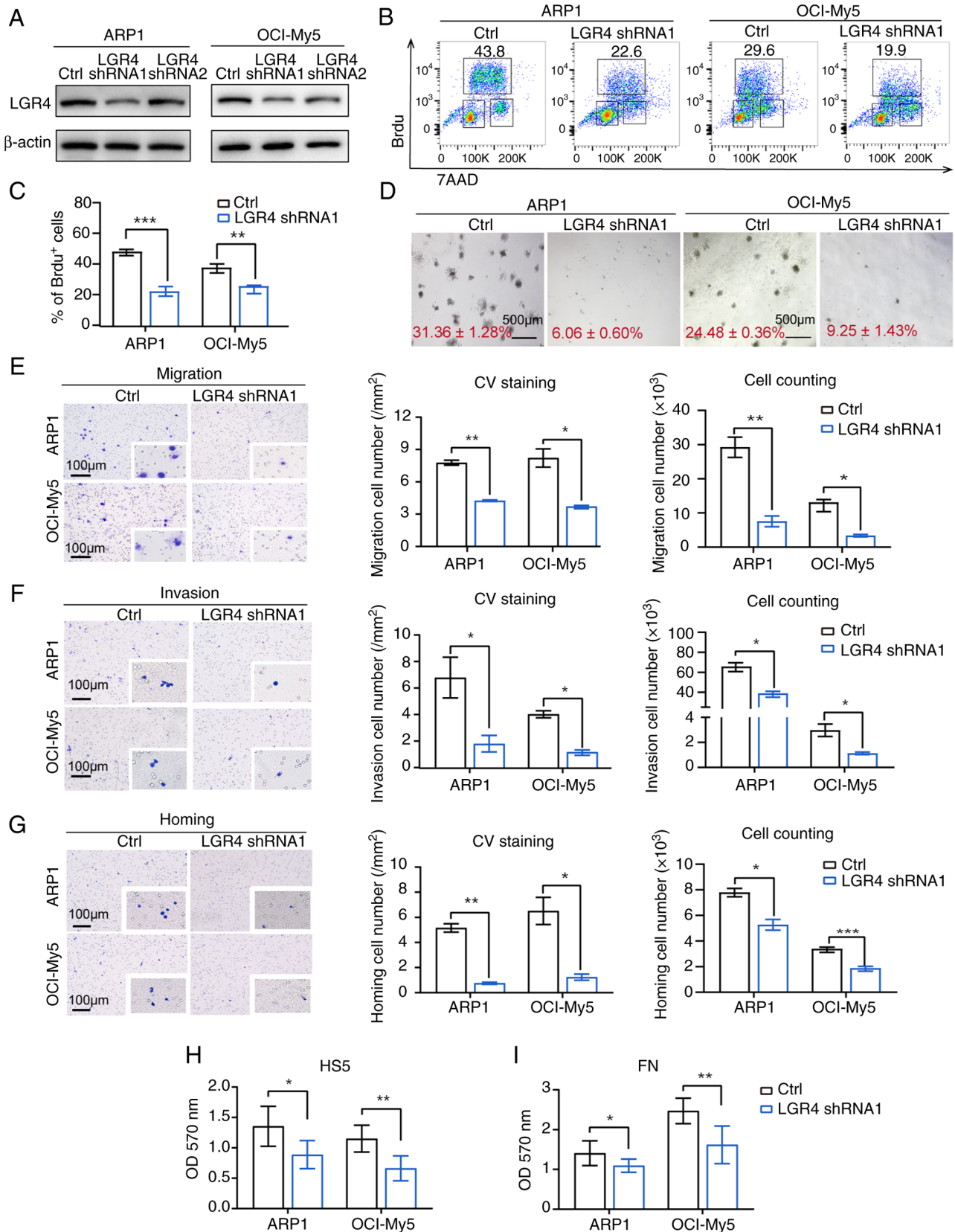
Figure 3. LGR4 knockdown impairs cell proliferation, adhesion, migration and homing in MM cells *in vitro*. (A) Western blots of LGR4-silencing in ARP1 and OCI-My5, compared with the controls. (B) Representative flow cytometry dot plots for detection of BrdU-positive cells. (C) Statistical analysis of the number of BrdU-positive cells among LGR4-silencing MM cells. (D) Representative images of clonogenic analysis in ARP1-Ctrl, ARP1-LGR4-shRNA1, OCI-Ctrl and OCI-LGR4-shRNA1 cells cultured in RPM1-1640 media. Scale bars, 500 μm. (E) Transwell migration assays were conducted with LGR4-knockdown ARP1 and OCI-My5 cells. The quantification of the number of migratory cells is presented in the column graph. Scale bars, 100 μm. (F) Matrigel invasion assays were conducted with LGR4-knockdown ARP1 and OCI-My5 cells. The quantification of the number of invasive cells is illustrated in the column graph. Scale bars, 100 μm. (G) Cell homing assays were conducted with LGR4-knockdown ARP1 and OCI-My5 cells. Scale bars, 100 μm. (H) The quantification of the number of homing cells is presented in the column graph. (I) Adhesion assay of LGR4-knockdown ARP1 and OCI-My5 co-cultured with HS5 cells or FN. Statistical analyses were performed using Student's t-test. *P<0.05, **P<0.01 and ***P<0.001. MM, multiple myeloma; shRNA, short hairpin RNA.
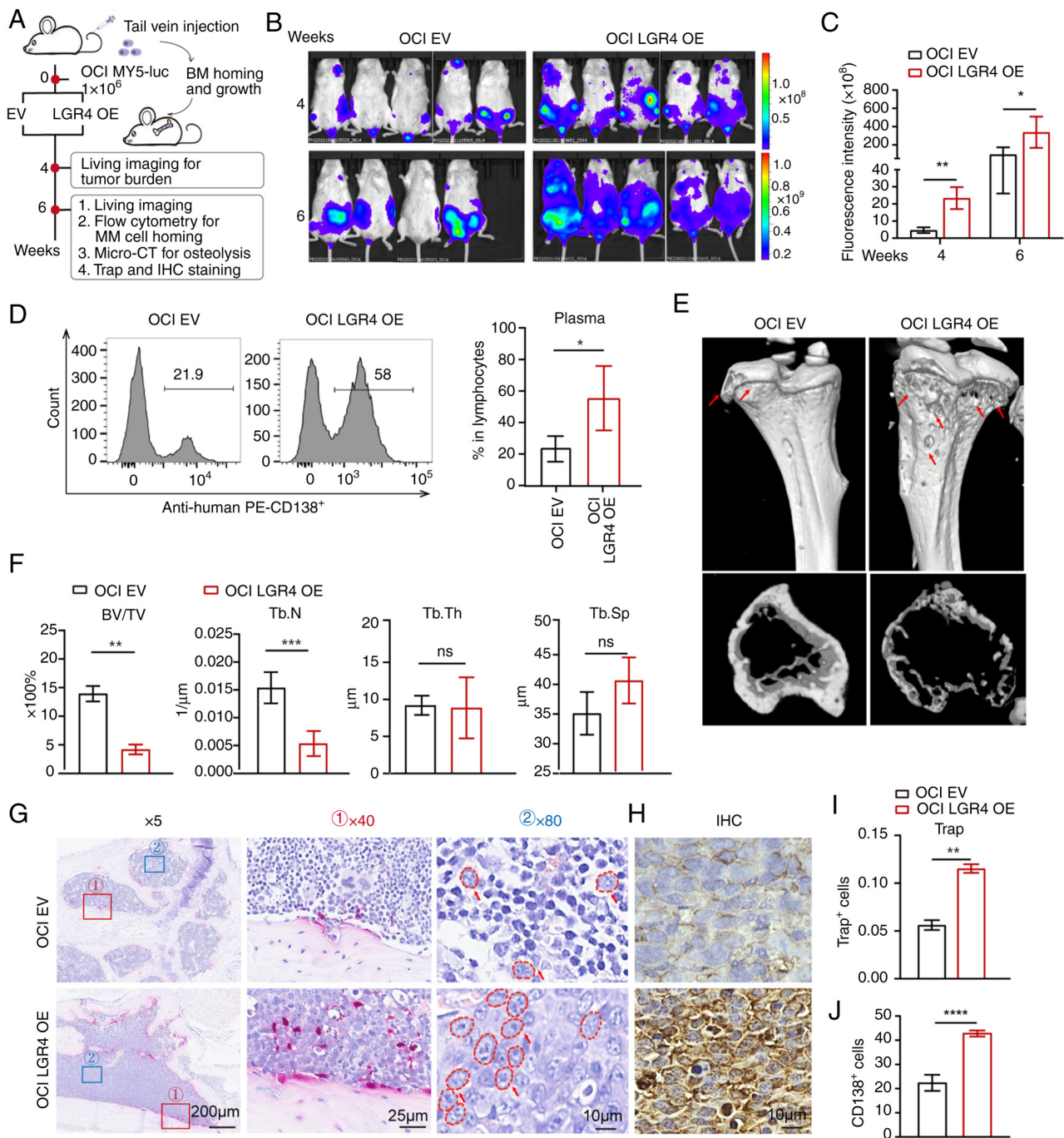
Figure 4. Overexpression of LGR4 promotes cells' homing to the BM and MM progression *in vivo*. (A) Schematic of *in vivo* experiments. (B) Tumor-associated live imaging of NCG mice injected with OCI-Ctrl or OCI-LGR4-OE cells at 4 and 6 weeks (n=5 for each group). (C) Quantification of luminescence intensity in live NCG mice. (D) Flow cytometric analysis images and statistics of the human MM cell proportion in the bone marrow after sacrificing NCG mice. (E) Micro-CT images of tibia derived from NCG mice. (F) Quantification of bone microstructural parameters, namely BV/TV, Tb.N, Tb.Th and Tb.Sp (n=3). (G) TRAP staining for NCG xenografted mice bone marrow section. Scale bars, 200, 25 and 10 μm. (I) The quantification of the number of Trap-positive osteoclast cells is presented in the column graph. (H) Neoplastic CD138-positive plasma cells. Scale bars, 10 μm. (J) The quantification of the number of neoplastic CD138 positive plasma cells is presented in the column graph. Statistical analyses were performed using Student's t-test. $^{*}P<0.05$, $^{**}P<0.01$, $^{***}P<0.001$ and $^{****}P<0.0001$. BM, bone marrow; MM, multiple myeloma; LGR4-OE, LGR4 overexpression; BV/TV, trabecular bone volume fraction; Tb.N, trabecular number; Tb.Th, trabecular thickness; Tb.Sp, trabecular separation; TRAP, tartrate-resistant acid phosphatase; EV, empty vector; ns, not significant (P>0.05).

the signaling pathways regulated by LGR4 in MM, RNA-seq was performed on OCI-LGR4-OE and OCI-LGR4-shRNA1, along with the control cells. Moreover, GSEA exhibited major types of gene signatures in LGR4-OE cells that were enriched in the regulation of cell migration and cell adhesion (Figs. 5A-C, S5A and B). Then, the changes in the expression of key cell-adhesion genes were verified at both mRNA and protein levels, including N-Cadherin, Snail, Vimentin, MUC2, ZEB1, TNFRSF1B in LGR4-OE, LGR4-shRNA1 in ARP1 and OCI-My5 cells (Figs. 5D and E and S5C). The results indicated that LGR4-OE significantly increased the cell-adhesion molecules while LGR4-knockdown resulted in a significant decrease (Figs. 5F and G and S5D). A recent study has suggested that LGR4 regulates intestinal epithelial
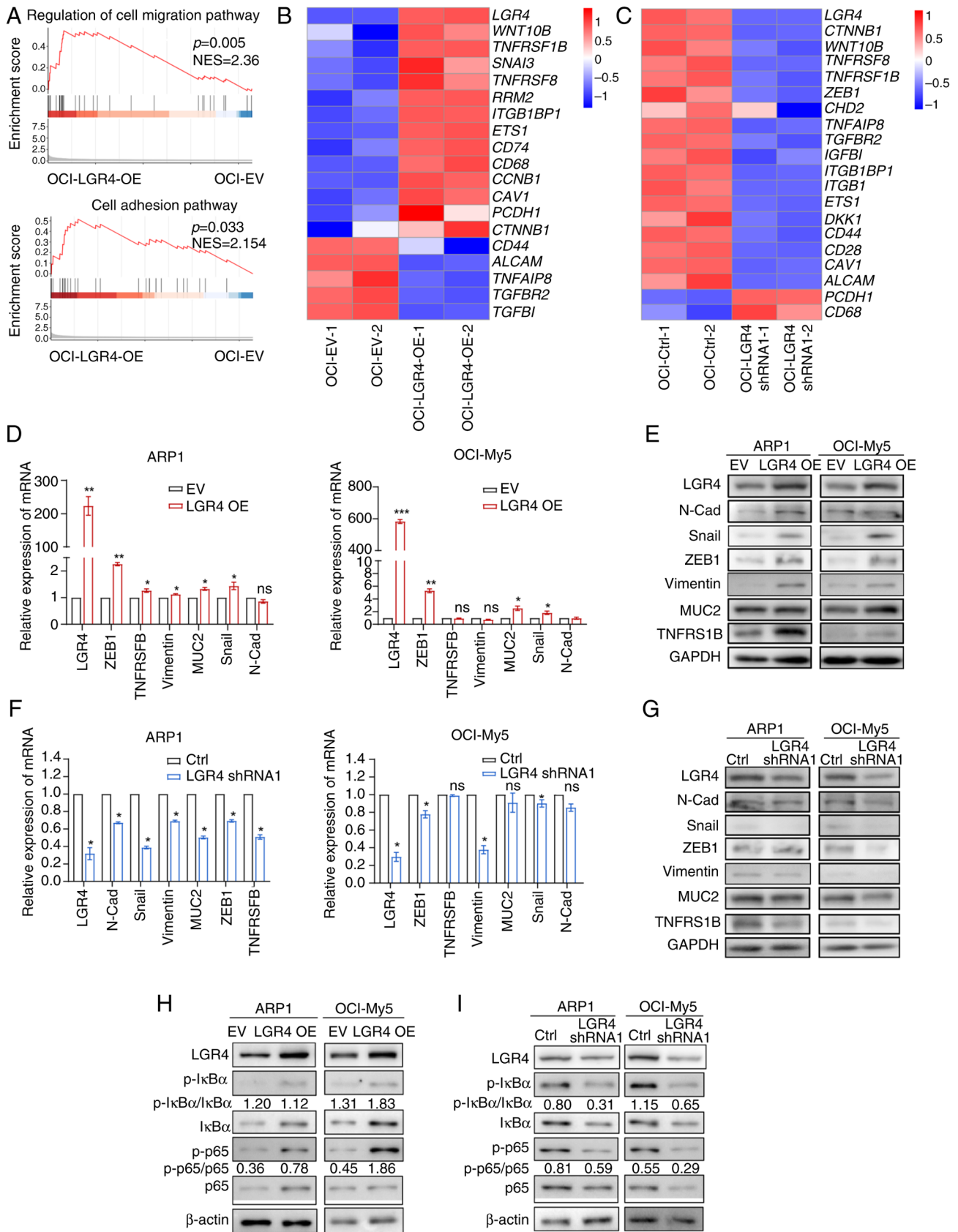
Figure 5. Cell-adhesion association genes and NF-κB signaling pathway are upregulated in LGR4-OE multiple myeloma cells. (A) Gene Set Enrichment Analysis of cell-adhesion pathway-related genes from differentially expressed genes between OCI-Ctrl and OCI-LGR4-OE. (B and C) Heatmap of RNA sequencing analysis of adhesion-related gene expression in OCI-EV, OCI-LGR4-OE, OCI-Ctrl, and OCI-LGR4-shRNA1. (D and E) Relative mRNA and protein levels of cell-adhesion genes in OCI-EV and OCI-LGR4-OE cells, respectively. (F and G) Relative mRNA and protein levels of cell-adhesion genes in OCI-Ctrl and OCI-LGR4-shRNA1 cells, respectively. (H and I) The protein level of NF-κB signal genes was detected in (H) OCI-EV and OCI-LGR4-OE cells; and (I) in OCI-Ctrl and OCI-LGR4-shRNA1 cells (I). Statistical analyses were performed using Student's t-test. [*]P<0.05, [**]P<0.01 and [***]P<0.001. LGR4-OE, LGR4 overexpression; EV, empty vector; shRNA, short hairpin RNA; p-, phosphorylated; ZEB1, Zinc Finger E-Box Binding Homeobox 1; ns, not significant (P>0.05).

cell proliferation and development through C-terminal activation of NF-κB signaling (32). R-spondin signals drive NF-kB activity through LGR4 and stimulate the proliferation of stem cells (33). It has been reported that activated NF-κB signaling enhances the ability of hematopoietic stem cell homing (9). Besides, NF-κB signaling can activate endothelial cell adhesion molecules (34). Therefore, it was hypothesized that LGR4 promotes MM cell homing by activating NF-κB signaling. To investigate whether LGR4 influences MM cell adhesion through NF-κB activation, the protein level of key NF-κB genes was determined, including p65, phosphorylated (p-)p65, IκBα and p-IκBα. The results indicated that LGR4-OE significantly activated NF-κB signaling, while LGR4-knockdown decreased as western blotting illustrated (Figs. 5H and I, S5E and F). The aforementioned data indicate that LGR4 promotes cell homing to BM through activating NF-κB signaling.

Inhibition of NF-κB pathway suppresses cell homing and MM progression in vitro. It was further investigated whether QNZ, an NF-κB signaling pathway inhibitor, could suppress cell proliferation and homing in MM. The IC$_{50}$ of QNZ was significantly lower in LGR4-OE ARP1 and OCI-My5 cells compared with the control group (Fig. 6A). Growth curves indicated that the proliferation was inhibited in the LGR4-OE cells treated with QNZ (Fig. S6C and E). Cell cycle assays exhibited that QNZ alleviated the increased proportion of S-phase cells caused by the overexpression of LGR4 in ARP1 and OCI-My5 cells (Fig. 6B). Subsequently, to investigate whether QNZ inhibits LGR4-induced cell adhesion and homing, Transwell assay of cell homing was performed. The results revealed that cell homing ability induced by LGR4-OE was inhibited after 48 h of QNZ treatment (Figs. 6C and D). Additionally, the Transwell migration and Matrigel invasion assays confirmed that QNZ reduced cell migration and invasion of cells, with the quantification of migratory cells supporting these results (Figs. 6F and G, and S6A and B). Consistently, the results of the cell co-culture adhesion assay exhibited that MM cell adhesion ability was reduced after 48 h of QNZ treatment in LGR4-OE ARP1 and OCI-My5 cells (Fig. 6H and I). Furthermore, western blot analysis revealed that QNZ treatment significantly inhibited NF-κB signaling in LGR4-OE cells, with a corresponding decrease in the expression of adhesion-associated molecules ZEB1 (Figs. 6J, S6D and F). As a critical function subunit of NF-κB signal, *RELA* (p65) contains transcriptional activation domains of gene transcription and facilitates the binding of p50 to DNA (35,36). Subsequently, to verify interaction molecules of NF-κB signaling activation by LGR4, siRNA was used to knock down *RELA* in LGR4-OE MM cells. Protein levels (Fig. S7A and B) confirmed a significant knockdown of *RELA* in LGR4-OE ARP1 and OCI-My5 cells, compared with the same cell lines transduced with SiNC serving as controls. The results indicated that siRNA1 and siRNA3 were more pronounced. Knockdown of RELA reversed the LGR4-induced proliferation and homing effects, as demonstrated by growth curve analysis (Fig. S7C), cell cycle assays (Fig. S7D), Transwell analysis about cell homing (Fig. S7E and F) and migration (Fig. S7G and H). By activating the NF-κB pathway, LGR4 facilitates the entry of the p50/RELA dimer into the nucleus to initiate gene transcription. The aforementioned results

confirmed that inhibition of the NF-κB pathway alleviated the promoting effect of LGR4-OE on adhesion ability and MM cell homing to BM.

Inhibition of the NF-κB pathway relieves the effect of LGR4-OE on MM cell proliferation and cell homing in vivo. To explore whether QNZ has similar effects *in vivo* as observed *in vitro*, 1x10^6 OCI-ctrl and OCI-LGR4-OE cells were injected through the tail vein into NCG mice to establish a xenografts mouse model. A total of 10 days post-transplantation, QNZ was injected intraperitoneally every two days (Fig. 7A). As compared with the solvent-treated mice (Fig. 7B), the mice treated with QNZ exhibited a reduction in tumor-associated luminescence intensity in the LGR4-OE group at weeks 3 and 6 (Fig. 7C). Due to reaching the humane endpoint at week 6, one mouse from each in the solvent group was observed to exhibit paralysis, then succumbed unexpectedly the following day, therefore the mice were euthanized. To verify whether QNZ affected cell homing, femur and tibia were dissected for image of bone tissue. The fluorescence intensity in the bone of the LGR4-OE group was higher, whereas QNZ treatment significantly reduced this intensity, particularly in the LGR4-OE group (Fig. 7D and E). Flow cytometric analysis confirmed that QNZ treatment significantly decreased the proportion of human MM cells in the BM of LGR4-OE mice compared with the solvent group (Fig. 7F and G).

Next, micro-CT scanning was used to detect bone damage in the tibia, revealing that QNZ treatment rescued severe trabecular bone loss caused by LGR4-OE, compared with the solvent-treated mice (Figs. 7J). Quantitative analysis of bone microstructure parameters exhibited that both Tb.BV/TV and Tb.N were improved (Fig. 7H). TRAP staining revealed that the number of osteoclasts was reduced in QNZ-treated LGR4-OE mice in contrast to solvent mice (Fig. 7K). Quantitative analysis of TRAP-positive osteoclast cells confirmed this reduction (Fig. 7I). In summary, these results demonstrated that inhibition of the NF-κB pathway relieves the effects of LGR4 overexpression on MM cell proliferation and cell homing *in vivo*.

Discussion

The interaction between MM cells and BMME is essential to MM malignant proliferation and bone destruction (4,5). The present study provides direct evidence, using genetic approaches, that LGR4 plays a critical role in regulating MM cell proliferation, migration and homing. Mechanistically, it was demonstrated that elevated LGR4 expression in MM cells activates the NF-κB signaling pathway and upregulates the migration-related adhesion molecule ZEB1, thus facilitating MM cell homing into BM (Fig. 8). Exploring the role of LGR4 in cell homing and tumorigenesis offers valuable insights into the molecular evolution of MM, which is vital for optimizing both current and future treatment strategies.

The physiological role of LGR4 is associated with the development of multiple organs. LGR4-deficient mice exhibit developmental defects in various organs, including the eyes, bones and reproductive system (10-13). Our previous study demonstrated that LGR4 plays a role in early hematopoietic cell differentiation (9). Under pathological conditions,
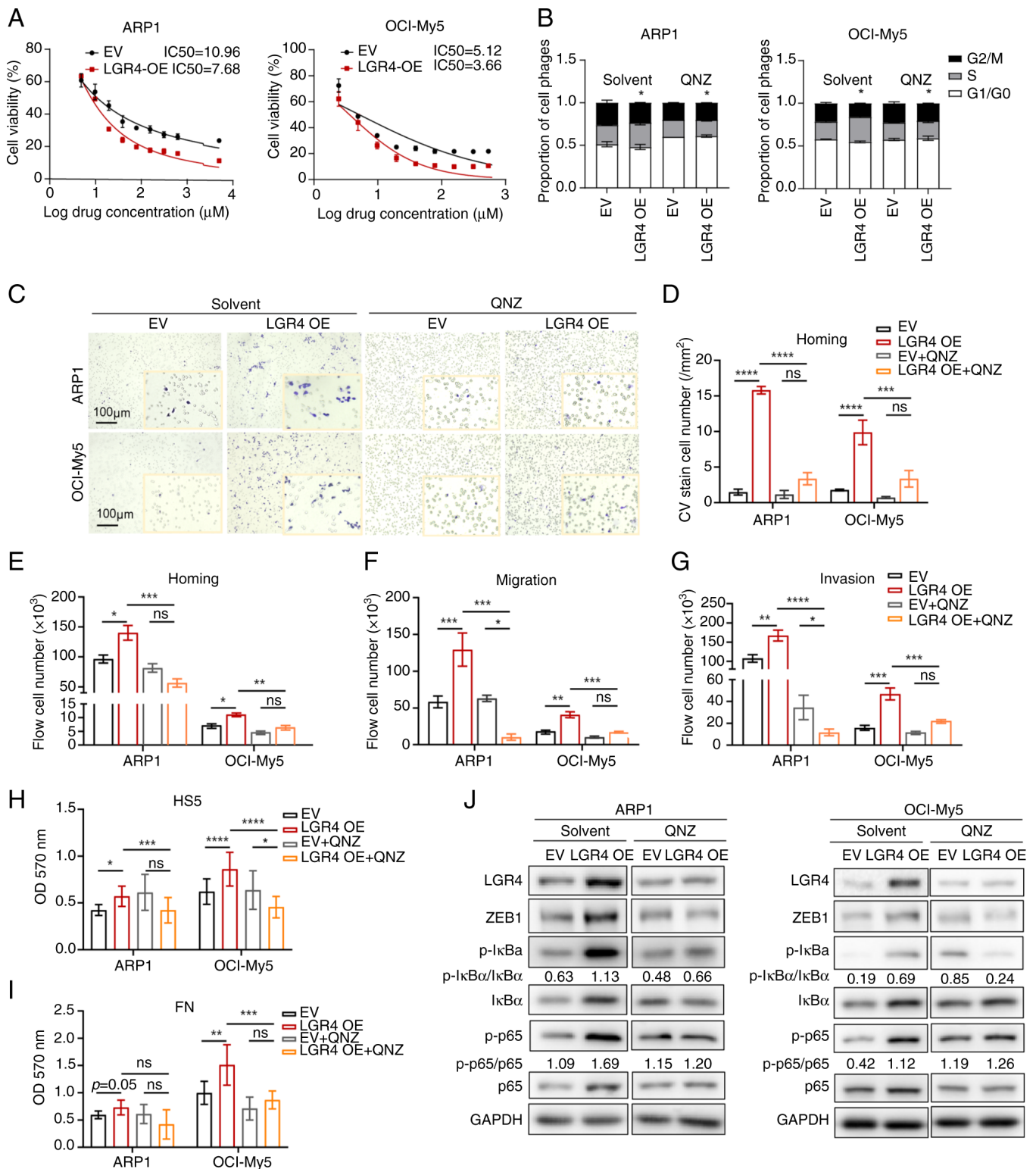
Figure 6. Inhibition of NF-κB pathway suppresses cell homing and multiple myeloma progression *in vitro*. (A) IC_{50} test with Cell Counting Kit-8 assays of LGR4-OE ARP1 and OCI-My5 cells after treatment with doubling dilution of QNZ (0-2,500 nmol/l, doubling dilution). (B) The proportions of cell cycle phases in LGR4-OE ARP1 and OCI-My5 cells with the addition of solvent or QNZ treatment for 48 h. (C-E) Cell homing assays were conducted with LGR4-OE ARP1 and OCI-My5 cells after solvent or QNZ treatment for 48 h. Scale bars, 100 µm. The quantification of the number of homing cells is presented in the column graph. (D-G) The quantification of the (D and E) homing, (F) migration and (G) invasion cell count with LGR4-OE ARP1 and OCI-My5 cells after QNZ treatment. (H and I) Adhesion assay of LGR4-OE ARP1 and OCI-My5 cells after QNZ treatment co-cultured with (H) HS5 cells or (I) fibronectin. (J) Western blotting of NF-κB signal genes in LGR4-OE ARP1 and OCI-My5 cells after QNZ treatment. Statistical analyses were performed using two-way ANOVA with Tukey's post-hoc test. *P<0.05, **P<0.01, ***P<0.001 and ****P<0.0001. LGR4-OE, LGR4 overexpression; EV, empty vector; ns, not significant (P>0.05).

aberrant RSPO3-LGR4 signaling enhances tumor aggressiveness through increased epithelial-mesenchymal transition (EMT) in lung adenocarcinomas (37,38). Moreover, LGR4 facilitates breast cancer cell metastasis (15), which is an
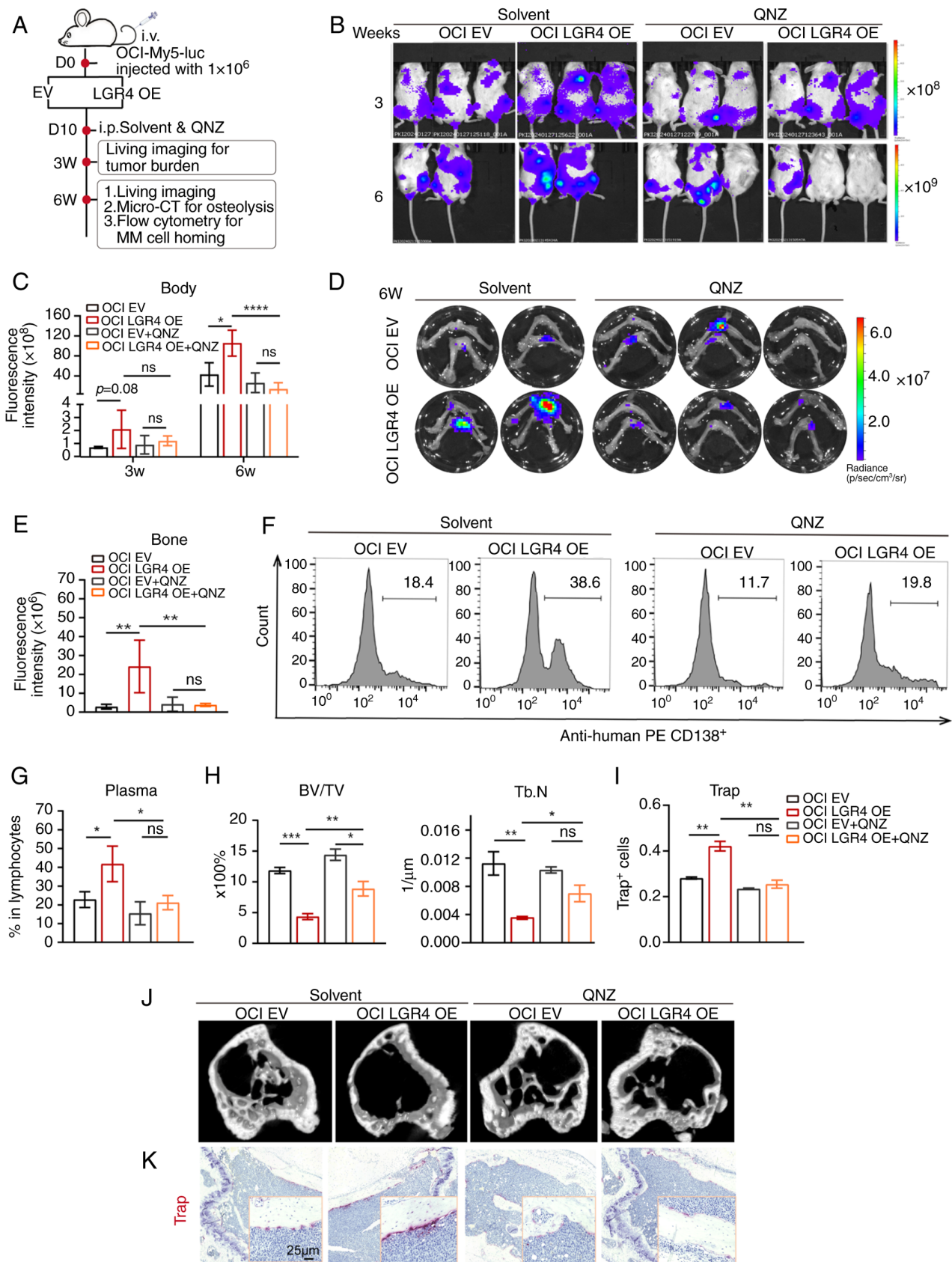
Figure 7. Inhibition of the NF-κB pathway relieves the effect of LGR4-OE on MM cell proliferation and cell homing *in vivo*. (A) Schematic of *in vivo* experiments (n=3 for each group). (B) Tumor-associated live imaging of NCG mice injected with OCI-Ctrl or OCI-LGR4-OE cells treated with solvent and QNZ (0.6 mg/kg) at 3 and 6 weeks. (C) Quantification of luminescence intensity in live NCG mice. (D) Tumor cell homing-associated living image in the bone marrow. (E) Quantification of luminescence intensity. (F and G) Flow cytometric analysis and statistics of the human MM cell proportion in the bone marrow. (H) Quantification of bone microstructural parameters, namely BV/TV and Tb.N (n=3). (I) Quantification of the number of TRAP positive osteoclast cells is illustrated in the column graph. (J) Micro-CT images of femurs derived from NCG mice. (K) representative TRAP staining for NCG mice bone marrow section treated with solvent and QNZ. Scale bars, 25 µm. Statistical analyses were performed using Student's t-test. $^*P<0.05$, $^{**}P<0.01$, $^{***}P<0.001$ and $^{****}P<0.0001$. LGR4-OE, LGR4 overexpression; MM, multiple myeloma; EV, empty vector; i.v., intravenously; ns, not significant (P>0.05).
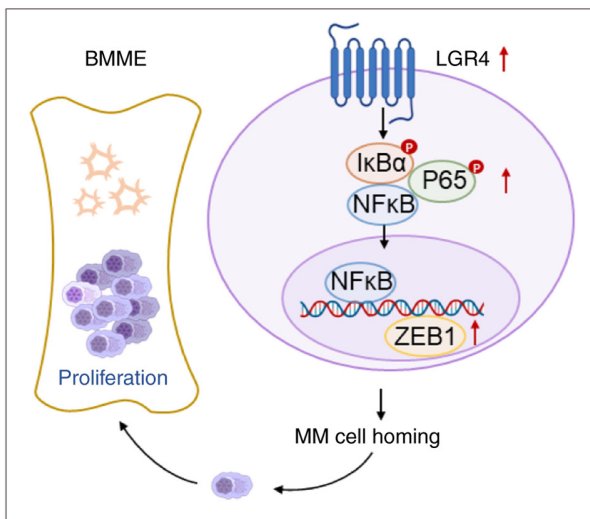
Figure 8. Schematic diagram of the current working hypothesis. MM, multiple myeloma; BMME, bone marrow microenvironment; ZEB1, Zinc Finger E-Box Binding Homeobox 1.

essential self-renewal gene in leukemia stem cells (39). Consistently, studies indicated that aberrant R-spondin/LGR4 signaling contributes to MM progression (16,17). In the present study, it was first demonstrated that the high expression of LGR4 associated significantly with myeloma cell homing, promoted bone destruction, and contributed to malignant progression in patients with MM using clinical information analysis. Furthermore, the current study confirms that LGR4 significantly enhances MM cell homing *in vitro* and exacerbates osteolytic bone destruction *in vivo*.

Normally, LGR4 has been reported to promote tumor progression through the activation of the Wnt signaling pathway. LGR4 activates Wnt-β catenin, which promotes EMT in lung cancer (37), and activates GSK3β to support tumor stem cell survival in acute myeloid leukemia (38). Additionally, LGR4 promoted aberrant MM proliferation through Wnt signaling (data not shown). Previous studies have demonstrated that NF-κB signaling enhances the homing ability of hematopoietic stem cells (18) and activates endothelial cell adhesion molecules (34). In the present study, the GSEA analysis revealed that regulating the cell migration pathway was enriched in RNA-seq data from LGR4-OE cells. It was observed that LGR4 overexpression activates the NF-κB signaling pathway and upregulates the migration-related adhesion molecule ZEB1, thereby promoting MM cell homing and tumor progression. Treating MM cells with an NF-κB inhibitor suppressed tumor progression, proliferation, cell migration and homing. Furthermore, the inhibitor's effective concentration at the nanomolar level presents significant potential for clinical translation. siRNA was used to suppress the expression of RELA (which encodes p65) to validate the results obtained from the NF-κB inhibitor in LGR4-OE cells. In summary, these findings suggest that the NF-κB inhibitor QNZ impairs MM cell homing.

Moreover, it was found that LGR4 expression was significantly correlated with the proportion of plasma cells in the BM and the number of MRI-defined focal lesions (40) that established a clinical correlation. Elevated LGR4 expression can serve as an early indicator of aggressive MM associated with severe bone fractures. Furthermore, LGR4, as a G-protein-coupled membrane receptor, suggests it could be a potential therapeutic target in MM. Recently, a humanized monoclonal antibody was developed, LGR4-mAb, which effectively inhibits LGR4/Wnt signaling by blocking LGR4 (14). The aforementioned antibody has been investigated for the treatment of colorectal cancer. Consequently, conjugating a monoclonal antibody targeting LGR4 with a proteasome inhibitor could be a promising approach for further investigation in MM. However, due to the structural diversity and the cross-reactivity of similarity receptors such as LGR5/6, the limitation of the use of anti-LGR4 antibodies may overcome by focus on improving binding affinity (41,42). The present findings suggest that targeting LGR4 holds significant potential as a therapeutic strategy for inhibiting MM progression.

Since LGR4 is recognized as a key regulator of osteoblast and osteoclast differentiation (8), its high expression in MM can be correlated with osteoclast differentiation, promoting MM progression by inducing bone disease. The role of highly expressed LGR4 on MM cells and the tumor microenvironment, such as the possible promotion of MM bone disease by promoting osteoclast differentiation, remains to be further explored. Additionally, NF-κB inhibitors can suppress MM cell proliferation and homing and can be tested in combination with frequently used clinical therapies, including proteasome inhibitors, to evaluate their therapeutic efficacy. The current findings reveal that LGR4 influences MM by activating NF-κB, as shown in the use of NF-κB inhibitors and RELA knockdown. The specific molecules and mechanisms involved in LGR4-mediated NF-κB signaling remain to be fully elucidated. Therefore, the potential role and mechanism of LGR4 in MM require further investigation.

In conclusion, it was demonstrated that the elevated LGR4 contributes to MM progression by modulating cell adhesion, thereby promoting cell homing to BM. LGR4 activates NF-κB signaling, which enhances cell homing. The findings of the present study suggest that targeting LGR4 holds significant potential as a therapeutic strategy for inhibiting MM progression.

Acknowledgements

Funding

Availability of data and materials

The data generated in the present study are included in the figures and/or tables of this article. The data generated in the present study may be found in the National Genomics Data Center under accession number HRA007584 or at the following URL: https://ngdc.cncb.ac.cn/search/specific?db=hra&q=HRA007584.

Authors' contributions

WZ and GZ designed the study. NH, ZL and XL performed experiments and analyzed the data. ZL and FS collected clinical samples. QY, JG, CK, YZ, XC, GA and XF provided technical assistance. WZ and NH wrote and revised the manuscript. WZ, NH and QY confirm the authenticity of all the raw data. All authors read and approved the final version of the manuscript.

Ethics approval and consent to participate

For using human samples, the Cancer Research Institute Review Board of Central South University (Changsha, China) approved the present study (date, 2019/03/12; approval no. 2022-KT188). All patients provided written informed consent. All animal experiments were performed in accordance with the guidelines of the Institutional Animal Care and local Veterinary Office and Ethics Committee of the Animal Center of Hunan Normal University School of Medicine (approval no. D2021013; Changsha, China).

Patient consent for publication

Not applicable.

Competing interests

The authors declare that they have no competing interests.

References

1. Palumbo A and Anderson K: Multiple myeloma. N Engl J Med 364: 1046-1060, 2011.
2. Slovak ML: Multiple myeloma: Current perspectives. Clin Lab Med 31: 699-724, 2011
3. Chauhan D, Uchiyama H, Akbarali Y, Urashima M, Yamamoto K, Libermann TA and Anderson KC: Multiple myeloma cell adhesion-induced interleukin-6 expression in bone marrow stromal cells involves activation of NF-kappa B. Blood 87: 1104-1112, 1996.
4. Neri P, Ren L, Azab AK, Brentnall M, Gratton K, Klimowicz AC, Lin C, Duggan P, Tassone P, Mansoor A, et al: Integrin β7-mediated regulation of multiple myeloma cell adhesion, migration, and invasion. Blood 117: 6202-6213, 2011.
5. Xu L, Mohammad KS, Wu H, Crean C, Poteat B, Cheng Y, Cardoso AA, Machal C, Hanenberg H, Abonour R, et al: Cell adhesion molecule CD166 drives malignant progression and osteolytic disease in multiple myeloma. Cancer Res 76: 6901-6910, 2016.
6. Kinzel B, Pikiolek M, Orsini V, Sprunger J, Isken A, Zietzling S, Desplanches M, Dubost V, Breustedt D, Valdez R, et al: Functional roles of Lgr4 and Lgr5 in embryonic gut, kidney and skin development in mice. Dev. Biol 390: 181-190, 2014.
7. Mao B, Huang S, Lu X, Sun W, Zhou Y, Pan X, Yu J, Lai M, Chen B, Zhou Q, et al: Early development of definitive erythroblasts from human pluripotent stem cells defined by expression of glycophorin A/CD235a, CD34, and CD36. Stem Cell Reports 7: 869-883, 2016.
8. Luo J, Yang Z, Ma Y, Yue Z, Lin H, Qu G, Huang J, Dai W, Li C, Zheng C, et al: LGR4 is a receptor for RANKL and negatively regulates osteoclast differentiation and bone resorption. Nat Med 22: 539-546, 2016.
9. Wang Y, Wang H, Guo J, Gao J, Wang M, Xia M, Wen Y, Su P, Yang M, Liu M, et al: LGR4, Not LGR5, enhances hPSC hematopoiesis by facilitating mesoderm induction via TGF-Beta signaling activation. Cell Rep 31: 107600, 2020.
10. Weng J, Luo J, Cheng X, Jin C, Zhou X, Qu J, Tu L, Ai D, Li D, Wang J, et al: Deletion of G protein-coupled receptor 48 leads to ocular anterior segment dysgenesis (ASD) through down-regulation of Pitx2. Proc Natl Acad Sci USA 105: 6081-6086, 2008.
11. Luo W, Rodriguez M, Valdez JM, Zhu X, Tan K, Li D, Siwko S, Xin L and Liu M: Lgr4 is a key regulator of prostate development and prostate stem cell differentiation. Stem Cells 31: 2492-2505, 2013.
12. Wang J, Liu R, Wang F, Hong J, Li X, Chen M, Ke Y, Zhang X, Ma Q, Wang R, et al: Ablation of LGR4 promotes energy expenditure by driving white-to-brown fat switch. Nat Cell Biol 15: 1455-1463, 2013.
13. Wu J, Xie N, Xie K, Zeng J, Cheng L, Lei Y, Liu Y, Song L, Dong D, Chen Y, et al: GPR48, a poor prognostic factor, promotes tumor metastasis and activates β-catenin/TCF signaling in colorectal cancer. Carcinogenesis 34: 2861-2869, 2013.
14. Zheng H, Liu J, Cheng Q, Zhang Q, Zhang Y, Jiang L, Huang Y, Li W, Zhao Y, Chen G, et al: Targeted activation of ferroptosis in colorectal cancer via LGR4 targeting overcomes acquired drug resistance. Nat Cancer 5: 572-589, 2024.
15. Yue Z, Niu X, Yuan Z, Qin Q, Jiang W, He L, Gao J, Ding Y, Liu Y, Xu Z, et al: RSPO2 and RANKL signal through LGR4 to regulate osteoclastic premetastatic niche formation and bone metastasis. J Clin Invest 132: e144579, 2022.
16. van Andel H, Ren Z, Koopmans I, Joosten SP, Kocemba KA, de Lau W, Kersten MJ, de Bruin AM, Guikema JE, Clevers H, et al: Aberrantly expressed LGR4 empowers Wnt signaling in multiple myeloma by hijacking osteoblast-derived R-spondins. Proc Natl Acad Sci USA 114: 376-381, 2017.
17. Yi Z, Ma T, Liu J, Tie W, Li Y, Bai J, Li L and Zhang L: LGR4 promotes tumorigenesis by activating TGF-β1/Smad signaling pathway in multiple myeloma. Cell Signal 110: 110814, 2023.
18. Huang X, Guo B, Liu S, Wan J and Broxmeyer HE: Neutralizing negative epigenetic regulation by HDAC5 enhances human haematopoietic stem cell homing and engraftment. Nat Commun 9: 2741, 2018.
19. Rajkumar SV, Dimopoulos MA, Palumbo A, Blade J, Merlini G, Mateos MV, Kumar S, Hillengass J, Kastritis E, Richardson P, et al: International Myeloma Working Group updated criteria for the diagnosis of multiple myeloma. Lancet Oncol 15: e538-e548, 2014.
20. Zhang J, Shi F, Liu X, Wu X, Hu C, Guo J, Yang Q, Xia J, He Y, An G, et al: Proline promotes proliferation and drug resistance of multiple myeloma by downregulation of proline dehydrogenase. Br J Haematol 201: 704-717, 2023.
21. Noborio-Hatano K, Kikuchi J, Takatoku M, Shimizu R, Wada T, Ueda M, Nobuyoshi M, Oh I, Sato K, Suzuki T, et al: Bortezomib overcomes cell-adhesion-mediated drug resistance through downregulation of VLA-4 expression in multiple myeloma. Oncogene 28: 231-242, 2009.
22. Xia J, Zhang J, Wu X, Du W, Zhu Y, Liu X, Liu Z, Meng B, Guo J, Yang Q, et al: Blocking glycine utilization inhibits multiple myeloma progression by disrupting glutathione balance. Nat Commun 13: 4007, 2022.
23. Tu Q, Liu C, Wu D, Wen Y, Wang H, Su P, Liu Y Ma F, Shi L and Zhou J: Establishment of the screening model for highly efficient generation of megakaryocytes and platelets from human pluripotent stem cells (in Chinese). Sci Sin Vitae 47: 1363-1374, 2017.
24. Wu T, Hu E, Xu S, Chen M, Guo P, Dai Z, Feng T, Zhou L, Tang W, Zhan L, et al: clusterProfiler 4.0: A universal enrichment tool for interpreting omics data. Innovation (Camb) 2: 100141, 2021.
25. Zhou W, Yang Y, Xia J, Wang H, Salama ME, Xiong W, Xu H, Shetty S, Chen T, Zeng Z, et al: NEK2 induces drug resistance mainly through activation of efflux drug pumps and is associated with poor prognosis in myeloma and other cancers. Cancer Cell 23: 48-62, 2013.
26. Takeyama Y, Sato M, Horio M, Hase T, Yoshida K, Yokoyama T, Nakashima H, Hashimoto N, Sekido Y, Gazdar AF, et al: Knockdown of ZEB1, a master epithelial-to-mesenchymal transition (EMT) gene, suppresses anchorage-independent cell growth of lung cancer cells. Cancer Lett 296: 216-224, 2010.

27. Cui H, Li Z, Chen S, Li X, Chen D, Wang J, Li Z, Hao W, Zhong F, Zhang K, *et al*: CXCL12/CXCR4-Rac1-mediated migration of osteogenic precursor cells contributes to pathological new bone formation in ankylosing spondylitis. Sci Adv 8: eabl8054, 2022.

28. Hu Y, Zhang Y, Ni CY, Chen CY, Rao SS, Yin H, Huang J, Tan YJ, Wang ZX, Cao J, *et al*: Human umbilical cord mesenchymal stromal cells-derived extracellular vesicles exert potent bone protective effects by CLEC11A-mediated regulation of bone metabolism. Theranostics 10: 2293-2308, 2020.

29. Holt RU, Baykov V, Rø TB, Brabrand S, Waage A, Sundan A and Børset M: Human myeloma cells adhere to fibronectin in response to hepatocyte growth factor. Haematologica 90: 479-488, 2005.

30. Gazitt Y, Fey V, Thomas C and Alvarez R: Bcl-2 overexpression is associated with resistance to dexamethasone, but not melphalan, in multiple myeloma cells. Int J Oncol 13: 397-405, 1998.

31. Bianchi G, Czarnecki PG, Ho M, Roccaro AM, Sacco A, Kawano Y, Gullà A, Samur AA, Chen T, Wen K, *et al*: ROBO1 promotes homing, dissemination, and survival of multiple myeloma within the bone marrow microenvironment. Blood Cancer Discov 2: 338-353, 2021.

32. Lai S, Cheng R, Gao D, Chen YG and Deng C: LGR5 constitutively activates NF-κB signaling to regulate the growth of intestinal crypts. FASEB J 34: 15605-15620, 2020.

33. Wizenty J, Müllerke S, Kolesnichenko M, Heuberger J, Lin M, Fischer AS, Mollenkopf HJ, Berger H, Tacke F and Sigal M: Gastric stem cells promote inflammation and gland remodeling in response to Helicobacter pylori via Rspo3-Lgr4 axis. EMBO J 41: e109996, 2022.

34. Takeuchi M and Baichwal VR: Induction of the gene encoding mucosal vascular addressin cell adhesion molecule 1 by tumor necrosis factor alpha is mediated by NF-kappa B proteins. Proc Natl Acad Sci USA 92: 3561-3565, 1995.

35. O'Shea JM and Perkins ND: Thr435 phosphorylation regulates RelA (p65) NF-kappaB subunit transactivation. Biochem J 426: 345-354, 2010.

36. Perkins ND: The diverse and complex roles of NF-κB subunits in cancer. Nat Rev Cancer 12: 121-132, 2012.

37. Gong X, Yi J, Carmon KS, Crumbley CA, Xiong W, Thomas A, Fan X, Guo S, An Z, Chang JT and Liu QJ: Aberrant RSPO3-LGR4 signaling in Keap1-deficient lung adenocarcinomas promotes tumor aggressiveness. Oncogene 34: 4692-4701, 2015.

38. Yue F, Jiang W, Ku AT, Young AIJ, Zhang W, Souto EP, Gao Y, Yu Z, Wang Y, Creighton CJ, *et al*: A Wnt-independent LGR4-EGFR signaling axis in cancer metastasis. Cancer Res 81: 4441-4454, 2021.

39. Salik B, Yi H, Hassan N, Santiappillai N, Vick B, Connerty P, Duly A, Trahair T, Woo AJ, Beck D, *et al*: Targeting RSPO3-LGR4 signaling for leukemia stem cell eradication in acute myeloid leukemia. Cancer Cell 38: 263-278.e6, 2020.

40. Mitchell JS, Li N, Weinhold N, Försti A, Ali M, van Duin M, Thorleifsson G, Johnson DC, Chen B, Halvarsson BM, *et al*: Genome-wide association study identifies multiple susceptibility loci for multiple myeloma. Nat Commun 7: 12050, 2016.

41. Stevens PD and Williams BO: LGR4: Not just for Wnt anymore? Cancer Res 81: 4397-4398, 2021.

42. Cowan AJ, Green DJ, Kwok M, Lee S, Coffey DG, Holmberg LA, Tuazon S, Gopal AK and Libby EN: Diagnosis and management of multiple myeloma: A review. JAMA 327: 464-477, 2022.